J. Fluid Mech. (2025), *vol.* 1014, A7, doi:10.1017/jfm.2025.10315

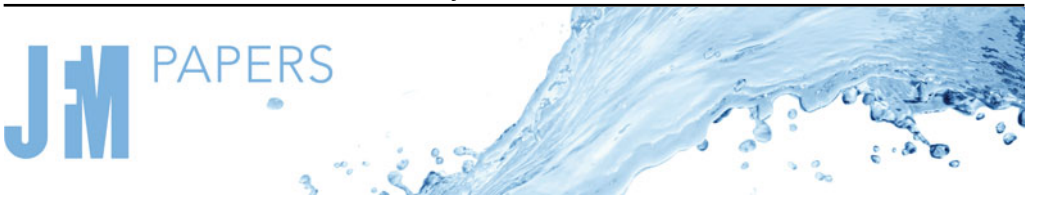

A framework for suppressing triad interaction in nonlinear dynamical systems: application to multiple states in two-dimensional Rayleigh–Bénard convection

Rikhi Bose[1] **and Xiaojue Zhu**[1]

[1]Max Planck Institute for Solar System Research, 37077 Göttingen, Germany

Corresponding authors: Xiaojue Zhu, zhux@mps.mpg.de; Rikhi Bose, rikhi.bose@gmail.com

(Received 20 January 2025; revised 21 May 2025; accepted 29 May 2025)

Nonlinear dynamical systems often allow for multiple statistically stationary states for the same values of the control parameters. Herein, we introduce a framework that selectively eliminates specific nonlinear triad interactions, thereby suppressing emergence of a particular state, and enabling the emergence of another. The methodology is applied to yield the multiple convection-roll states in two-dimensional planar Rayleigh–Bénard convection (e.g. Wang *et al.,* 2020, *Phys. Rev. Lett.*, vol. 125, 074501) in the turbulent regime. The intrusive framework presented here is based on the observation that the characteristic wavenumber associated with the mean horizontal size of the convection rolls mediates triadic scale interactions resulting in both kinetic energy and temperature variance cascades that are dominant energy transfer processes in a statistically stationary state. Suppression of these cascades mediated by a candidate wavenumber hinders the formation of the convection rolls at that wavenumber. Consequently, convection rolls are formed at another candidate wavenumber which is allowed to mediate energy to establish the cascade processes. In case no stable convection-roll states are possible, this technique does not tend to yield any convection rolls, making it a suitable method for discovering multiple states. Whereas in previous investigations the signature of different states in the initial condition in simulations yielded the multiple states, the present method alleviates such dependence of the emergence of multiple states on initial conditions. It is also demonstrated that accurate predictions of statistical quantities, such as Nusselt number and volume-averaged Reynolds numbers, can also be obtained using this method. The convection-roll states yielded using this technique may be used as initial conditions for direct simulations quickly converging to the target roll state without taking long convergence routes involving state transitions. Additionally, because only one state can

possibly emerge in each simulation, this technique can empirically designate each of the multiple states with respect to their stability.

Key words: Bénard convection, buoyancy-driven instability, turbulence theory

1. Introduction

Nonlinear dynamical systems often undergo state transitions as the control parameters are changed. Such bifurcations are generally characterised numerically using bifurcation diagrams. For example, to obtain steady and periodic solutions of nonlinear systems, numerical bifurcation analyses are performed in phase diagrams spanned by control parameters (Dijkstra *et al.* 2014); the continuation methods have been preferred to find these bifurcation diagrams, for example in thermal convection problems, such as in inclined layer convection (ILC) (Reetz & Schneider 2020; Reetz, Subramanian & Schneider 2020) and in steady planar Rayleigh–Bénard convection (RBC) with side-wall effects (Boullé *et al.* 2022). The bifurcation studies may also reveal junction points in bifurcation diagrams at which two or more branches of solutions intersect, implying the coexistence of several statistically stationary states with different transport properties for the same control parameters. Such bifurcation junctions have been reported in both turbulent and non-turbulent flow regimes. In recent literature, these states have been referred to as the multiple states. Examples of such flows include Taylor–Couette flow (Huisman *et al.* 2014; van der Veen *et al.* 2016), both rotating RBC and non-rotating two-dimensional (2-D) RBC (Xi & Xia 2008; van der Poel *et al.* 2012; Wang *et al.* 2018; Favier, Guervilly & Knobloch 2019), double diffusive convection (Yang *et al.* 2020), rotating spherical Couette flow (Zimmerman, Triana & Lathrop 2011) and von Karman flow (Ravelet *et al.* 2004; Cortet *et al.* 2010; Faranda *et al.* 2017), as well as some geophysical flows (Broecker, Peteet & Rind 1985; Weeks *et al.* 1997; Schmeits & Dijkstra 2001; Li, Sato & Kageyama 2002). For discovering the multiple states without change in control parameters, scientists have relied on computer simulations designed to yield these states. In the present work, we present a simple yet efficient methodology to quickly uncover the possible multiple states for a chosen set of control parameters in the turbulent regime in an example flow configuration, i.e. 2-D RBC.

The RBC is a canonical flow configuration for thermal convection. Fluid entrapped between a heated bottom plate and a cooled top plate is driven by buoyancy in RBC (Bodenschatz, Pesch & Ahlers 2000; Ahlers, Grossmann & Lohse 2009; Chillà & Schumacher 2012; Schumacher & Sreenivasan 2020; Xia *et al.* 2023; Lohse & Shishkina 2024). Generally, the effect of buoyancy is modelled using the Boussinesq approximation. Large-scale superstructures of horizontal size much larger than the distance between the plates are prevalent in three-dimensional (3-D) RBC (Pandey, Scheel & Schumacher 2018; Stevens *et al.* 2018; Krug, Lohse & Stevens 2020), and multiple states with different transport properties have not been identified as such. On the other hand, large-scale convection rolls whose horizontal size is similar to the distance between the plates are a distinctive feature of 2-D RBC. Depending on the flow driving strength, multiple roll states with different mean aspect ratios (Γ_r) can be yielded. Wang *et al.* (2020) extensively explored 2-D planar RBC over a wide range of Rayleigh numbers ($10^7 \leqslant Ra \leqslant 10^{10}$) and Prandtl numbers ($1 \leqslant Pr \leqslant 100$) in computer simulations. They obtained multiple states with $2/3 \leqslant \Gamma_r \leqslant 4/3$; the lower limit is approached at larger Ra. They showed that the

range of Γ_r obtained in simulations is reliant on the balance between elliptic instability and viscous damping.

The multiple states captured by Wang *et al.* (2020) in their direct numerical simulations (DNS) depended on the aspect ratio of the initial roll states. In cases where Γ_r of the converged statistically stationary state was different from the initial state, the convergence routes involved long transitions between states. In addition, the use of an exhaustive set of initial conditions for the realisation of all possible states might not be possible in such a methodology. Herein, we propose a novel technique that eliminates specific triad interactions involving one or more characteristic wavenumbers corresponding to the desired roll size. Consequently, roll formation at the target wavenumbers is suppressed, encouraging roll formation at other candidate wavenumbers. The proposed methodology can capture a state significantly quicker than even the DNS initialised with a target roll state, and the convergence route does not include state transitions. As will be demonstrated in the paper, this method circumvents the dependence of the converged roll state on the initial condition. The converged flow statistics obtained for the multiple states using the proposed method, such as Nusselt number (Nu) and volume-averaged horizontal and vertical Reynolds numbers, are also found to be in very good agreement with those obtained from DNS.

The turbulent 2-D RBC system allows for multiple states for a particular set of control parameters, unlike most other previous studies of emerging states in thermal convection with change in control parameters. For example, the bifurcation studies of ILC by Reetz & Schneider (2020) and Reetz *et al.* (2020) obtained the different states in phase diagrams changing the control parameters. In their ILC system, Reetz *et al.* (2020) found that (see p. 3 therein): 'Complex temporal dynamics may be observed where invariant states coexist at equal values of the control parameters.' In the present work, we compute these multiple states in a turbulent regime, far above the critical point. A typical numerical continuation method is unable to obtain the multiple states in one go as one continues along a branch. As mentioned previously, Wang *et al.* (2020) obtained these states by guiding the solutions of the nonlinear system towards a target state by prescribing the signature of the target states in the initial conditions. In contrast, we obtain the solutions more quickly, and irrespective of the initial conditions, by manipulating the energy transfer processes in triad interactions. Other methods of triad decimation have been used previously in studies of homogeneous isotropic turbulence (Frisch *et al.* 2012; Buzzicotti *et al.* 2016; Lanotte, Malapaka & Biferale 2016). However, in the present work, we only eliminate certain interactions in chosen triads involving the candidate wavenumber for roll formation as the mediator to guide the solutions towards target states instead of decimating whole triads.

2. Methodology

In our flow configuration, the bottom wall is heated and the top wall is cooled, with the gravity vector pointing towards the heated bottom wall. The two walls are located at $z = 0$ and $z = H$, respectively, so that H is the length scale associated with the thermal energy input to the system. The free-fall time scale denoted by $t_f = \sqrt{H/\alpha g\, \Delta\mathcal{T}}$, where α is the thermal expansion coefficient, g is the magnitude of gravitational acceleration, and $\Delta\mathcal{T} = \mathcal{T}_b - \mathcal{T}_t$ is the temperature difference between the two plates, is the time scale associated with the problem. Consequently, the velocity scale used for non-dimensionalisation is $u_f = H/t_f$. The horizontal and wall-normal components of coordinates are $\boldsymbol{x} = (x, z)$, and velocity is $\boldsymbol{u} = (u, w)$.

The RBC is governed by the Oberbeck–Boussinesq equations (OBEs). Here, $\Delta\mathcal{T}$ is considered small so that the Boussinesq approximation is applicable. The following are

the non-dimensionalised forms of the OBEs governing velocity $\boldsymbol{u}$ and temperature $\mathcal{T}$:

$$\boldsymbol{\nabla}\cdot\boldsymbol{u}=0, \tag{2.1}$$

$$\partial_t\boldsymbol{u}+\boldsymbol{u}\cdot\boldsymbol{\nabla}\boldsymbol{u}=-\boldsymbol{\nabla}p+\sqrt{\frac{Pr}{Ra}}\,\boldsymbol{\nabla}^2\boldsymbol{u}+\mathcal{T}\hat{\boldsymbol{z}}+\boldsymbol{f}, \tag{2.2}$$

$$\partial_t\mathcal{T}+\boldsymbol{u}\cdot\boldsymbol{\nabla}\mathcal{T}=\frac{1}{\sqrt{Ra\,Pr}}\boldsymbol{\nabla}^2\mathcal{T}+f_{\mathcal{T}}. \tag{2.3}$$

In (2.2) and (2.3), $\boldsymbol{f}$ and $f_{\mathcal{T}}$ are suitably chosen forcing terms. For DNS, both $\boldsymbol{f}$ and $f_{\mathcal{T}}$ are 0. As discussed later, in § 2.2, for the presented method, the expressions for the forcing terms $\boldsymbol{f}$ and $f_{\mathcal{T}}$ are such that certain triad interactions are removed, suppressing the formation of convection rolls with chosen Γ_r.

The walls are impermeable where Dirichlet boundary conditions are applied for both $\mathcal{T}$ and $\boldsymbol{u}$. We consider only the no-slip boundaries so that $\boldsymbol{u}=0$. The boundary conditions for $\mathcal{T}$ are $\mathcal{T}=1$ at $z=0$, and $\boldsymbol{u}=\mathcal{T}=0$ at $z=1$. In the horizontal direction, a periodic boundary condition is applied for both $\mathcal{T}$ and $\boldsymbol{u}$.

The non-dimensional parameters associated with the system are the Prandtl number $Pr=\nu/\kappa$, where ν and κ are the kinematic viscosity and thermal diffusivity, respectively, and the Rayleigh number $Ra=g\alpha\,\Delta\mathcal{T}\,H^3/\nu\kappa$, denoting the relative strength of thermal driving with respect to viscous dissipation. Once statistical stationarity is achieved in the simulations, the thermal energy input to the system is balanced by the viscous dissipation. Heat transport balances the thermal dissipation. Shraiman & Siggia (1990) and Ahlers *et al.* (2009) derived the kinetic and thermal dissipation rates from the kinetic energy and temperature variance budget equations: respectively,

$$\langle u_z\mathcal{T}\rangle=\frac{1}{\sqrt{Ra\,Pr}}(Nu-1)=\langle\varepsilon\rangle=\left\langle\frac{1}{2}\sqrt{\frac{Pr}{Ra}}\,(\boldsymbol{\nabla}\boldsymbol{u}+\boldsymbol{\nabla}\boldsymbol{u}^{\mathrm{T}})^2\right\rangle, \tag{2.4}$$

$$\langle\varepsilon_{\mathcal{T}}\rangle=\left\langle\frac{1}{\sqrt{Ra\,Pr}}\,(\boldsymbol{\nabla}\mathcal{T})^2\right\rangle=\frac{1}{\sqrt{Ra\,Pr}}\,Nu. \tag{2.5}$$

In these expressions, $\langle\cdot\rangle$ indicates time and volume averaging, and ε and $\varepsilon_{\mathcal{T}}$ are viscous and thermal dissipation, respectively. The Nusselt number Nu is the dimensionless heat transport, which is an output of the system. We have also used volume averaging and time averaging, denoted by $\langle\cdot\rangle_V$ and $\langle\cdot\rangle_t$, respectively. Specifically, for performance measures, we define the volume-averaged Reynolds number $Re=\sqrt{Re_x^2+Re_z^2}$, where

$$Re_x=\sqrt{\langle u^2\rangle_V}\;H/\nu, \tag{2.6}$$

$$Re_z=\sqrt{\langle w^2\rangle_V}\;H/\nu. \tag{2.7}$$

2.1. *Numerical simulations*

In this paper, we perform calculations for two $[Ra,\,Pr]$ combinations, $[10^8,\,10]$ and $[10^9,\,3]$. The computational domain and grid resolutions of the present simulations are the same as those reported for their DNS for the chosen $[Ra,\,Pr]$ by Wang *et al.* (2020). Therefore, all simulations presented here are fully resolved as in the DNS. Simulations

are performed in a computational domain of aspect ratio $\Gamma = L_x/H = 8$, with $H = 1$, the distance between the two plates for both $[Ra, Pr]$ combinations considered. For $[Ra, Pr] = [10^8, 10]$, 2048×256 grid points are used in the horizontal and vertical directions, respectively, and 4096×512 grid points resolve the computational domain for $[Ra, Pr] = [10^9, 3]$. As suggested by Wang *et al.* (2020), the fastest way to capture the multiple states in DNS is to prescribe the convection rolls with the target aspect ratio in the initial conditions. If $n^{(i)}$ is the number of rolls in the initial state, then the prescribed initial velocity and temperature fields are

$$\boldsymbol{u} = [u(x, z), w(x, z)] = \left[\sin\left(\frac{n^{(i)}\pi x}{\Gamma}\right) \cos(\pi z)\,, -\cos\left(\frac{n^{(i)}\pi x}{\Gamma}\right) \sin(\pi z) \right], \tag{2.8}$$

$$\mathcal{T} = 1 - z. \tag{2.9}$$

The OBEs in (2.1)–(2.3) were solved using the pseudo-spectral code based on the Dedalus partial differential equation solving framework (Burns *et al.* 2020). For spatial discretisation, Fourier and Chebychev expansions were used in the x and z directions. For dealiasing, we utilise the '3/2' rule. Time integration was performed by the third-order four-stage combination of a diagonally implicit Runge–Kutta scheme and an explicit Runge–Kutta scheme (RK443 time stepper). Time snapshots were stored at a time interval of one free-fall time unit for a period of 500 free-fall time units for the proposed forcing methodology switching on the forcing terms in (2.2) and (2.3); this time frame was sufficient for yielding the multiple states. However, DNS for $[Ra, Pr] = [10^9, 3]$ initiated with the target roll states (2.8) and (2.9) did not converge to a statistically stationary state within that interval, and therefore had to be run longer.

2.2. *Definitions of $\boldsymbol{f}$ and $f_{\mathcal{T}}$: scale-to-scale energy transfer*

The forcing terms in (2.2) and (2.3) remain to be defined. These terms are defined based on the observation that the characteristic horizontal wavenumber associated with the mean horizontal size of the convection rolls (k_r, say) acts as the mediator in wavenumber triads involved in establishing essential energy cascade processes at a statistical stationary state. To elaborate on this point, we quantify the nonlinear interactions in OBEs in (2.1)–(2.3).

To quantify the scale-to-scale energy transfers among the streamwise wavenumbers due to nonlinear triadic scale interactions, first Fourier transforms are performed for the temperature and components of the velocity fields. Then, corresponding to each wavenumber $l(2\pi/L_x)$ (where l is the integer wavenumber) or physical length scale L_x/l, the inverse transform is performed, thus obtaining the following flow fields corresponding to each physical length scale in the physical space:

$$\mathcal{T}_l(x, z, t) = \hat{\mathcal{T}}(l, z, t) \exp\left(il\tfrac{2\pi}{L_x}x\right), \tag{2.10}$$

$$\boldsymbol{u}_l(x, z, t) = \hat{\boldsymbol{u}}(l, z, t) \exp\left(il\tfrac{2\pi}{L_x}x\right). \tag{2.11}$$

Now let us assume a triad $[k, p, m](2\pi/L_x)$, where, k, p and $m = k - p$ are the integer receiver, donator and mediator streamwise wavenumbers, respectively. In the rest of the paper, the aforementioned convention is used to express the wavenumbers involved in a triad. Favier, Silvers & Proctor (2014) defined the transfer functions quantifying the scale-to-scale energy transfer between donator p and receiver k, mediated

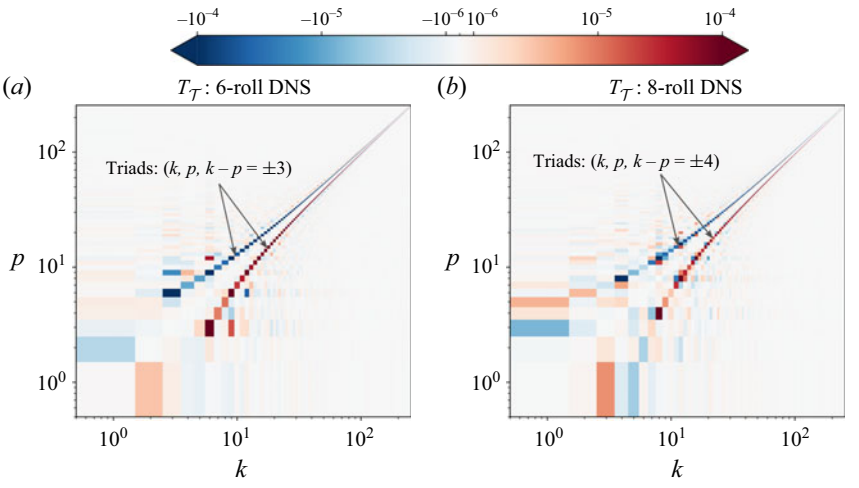

Figure 1. Scale-to-scale temperature variance transfer function $T_{\mathcal{T}}(k, p)$ from DNS of 2-D RBC at $[Ra, Pr] = [10^8, 10]$: (*a*) $n = 6$ state ($\Gamma_r = 4/3$), (*b*) $n = 8$ state ($\Gamma_r = 1$) (Bose *et al.* 2024). Here, k and p are the receiver and donator integer horizontal wavenumbers, respectively.

by the mediator $m = k - p$. The expressions for $T_{\mathcal{T}}(k, p)$, quantifying the scale-to-scale temperature variance transfer, and $T(k, p)$, quantifying the scale-to-scale kinetic energy transfer, are

$$T_{\mathcal{T}}(k, p) = -\int_V \mathcal{T}_k(\boldsymbol{u}_{k-p} \cdot \boldsymbol{\nabla} \mathcal{T}_p)\, \mathrm{d}V, \tag{2.12}$$

$$T(k, p) = -\int_V \boldsymbol{u}_k \cdot (\boldsymbol{u}_{k-p} \cdot \boldsymbol{\nabla} \boldsymbol{u}_p)\, \mathrm{d}V. \tag{2.13}$$

The integrands in the right-hand sides of (2.12) and (2.13) arise from the nonlinear advection terms of the OBEs, and are essentially the transport terms in the temperature variance and kinetic energy budget equations, respectively. For $T_{\mathcal{T}}(k, p) > 0$ ($T(k, p) > 0$), a positive amount of temperature variance (kinetic energy) is transferred from the donator wavenumber p to the receiver wavenumber k. Consequently, due to the principles of transactions, the transfer functions are anti-symmetric with respect to $k = p$, i.e. $T_{\mathcal{T}}(k, p) = -T_{\mathcal{T}}(p, k)$ and $T(k, p) = -T(p, k)$. The mediator wavenumber $k - p$ mediates the energy transfer process (Verma 2019; Bose, Kannan & Zhu 2024).

Bose *et al.* (2024) used the above expressions for scale-to-scale energy transfer functions (2.12) and (2.13) to study the dominant energy transfer processes in 2-D RBC. Their flow was for $[Ra, Pr] = [10^8, 10]$; of the multiple states, only the $\Gamma_r = 1$ state (here, $\Gamma_r = \Gamma/n = 1$, where n is the number of rolls in the converged state) was considered. Based on their DNS data, they showed that kinetic energy and temperature variance transfers between scales in a statistically stationary state are dominated by: (i) the energy transfer to/from the convection rolls, and (ii) the scale-to-scale kinetic energy and temperature variance cascades mediated by the convection rolls. These energy transfer processes are depicted here by plotting $T_{\mathcal{T}}(k, p)$ in figure 1, and $T(k, p)$ in figure 2, for the statistically stationary multiple states for $[Ra, Pr] = [10^8, 10]$. For this $[Ra, Pr]$ combination, Wang *et al.* (2020) found only two states – either $n = 6$ or $n = 8$ convection rolls were obtained, with mean aspect ratios $\Gamma_r = 4/3$ and 1, respectively.

For $T_{\mathcal{T}}(k, p)$, the scale-to-scale forward temperature variance cascade is the only dominant process (marked by arrows) for both cases in figure 1. This represents a forward

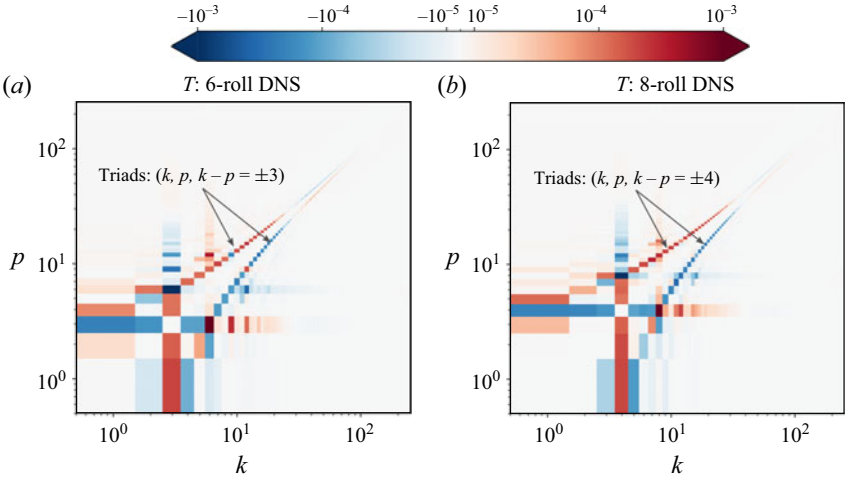

Figure 2. Scale-to-scale kinetic energy transfer function $T(k, p)$ from DNS of 2-D RBC at $[Ra, Pr] = [10^8, 10]$: (*a*) $n = 6$ state ($\Gamma_r = 4/3$), (*b*) $n = 8$ state ($\Gamma_r = 1$) (Bose *et al.* 2024). Here, k and p are the receiver and donator integer horizontal wavenumbers, respectively.

cascade because $T_{\mathcal{T}}(k, p) > 0$ for $k > p$ (the red patch), and the corresponding blue patch, where $T_{\mathcal{T}}(k, p) < 0$, corresponds to $p > k$: energy is transferred from larger scales to smaller scales. These two patches are positioned at a constant distance away from the line $k = p$ (the apparent curvature is due to the abscissa and the ordinate being plotted on logarithmic scale). Obviously, the separation is equal to the mediator wavenumber m, and the diagrams indicate it to be a constant. In fact, $m = k - p = \pm k_r$, where k_r is the characteristic integer wavenumber corresponding to the mean horizontal wavelength of the rolls, λ_r. For $n = 6$ and 8 states, $\lambda_r = 8/3$ and $8/4$, respectively, so that, $k_r = 3$ and 4 (as $k_r = L_x/\lambda_r$), respectively. Therefore, the triads involved in the process are of the form $[k, p, m = k - p = \pm k_r](2\pi/L_x)$. Clearly, the cascade process mediated by the rolls is essential for the sustenance of the statistically stationary state for both cases. Physically, the forward cascade is a consequence of an instability of the base flow comprising the convection rolls with characteristic wavenumber k_r.

In addition to the energy cascade process (marked by arrows), the energy transfers to/from the convection rolls are also relevant for scale-to-scale kinetic energy transfer process in figure 2 for both states. The cascade process is inverse in nature, i.e. $T(k, p) < 0$ for $k > p$ (the blue patch); energy transfer is from small scales to larger scales. As is for the temperature variance cascades in figure 1, the involved triads are of the form $[k, p, k - p = \pm k_r](2\pi/L_x)$. From these two figures, it becomes evident that the scale-to-scale energy cascades mediated by the convection rolls are crucial for their sustenance.

Similar analyses performed for the multiple states obtained for $[Ra, Pr] = [10^9, 3]$ also reveal that the convection rolls mediate energy in cascade processes. Wang *et al.* (2020) reported the existence of three states: $n = 8$ ($\Gamma_r = 1$), $n = 10$ ($\Gamma_r = 4/5$) and $n = 12$ ($\Gamma_r = 2/3$) convection rolls were obtained in a computational domain with aspect ratio $\Gamma = 8$. The temperature variance transfer function $T_{\mathcal{T}}(k, p)$ and kinetic energy transfer function $T(k, p)$ from DNS capturing these roll states are shown in figures 3 and 4, respectively. For $T_{\mathcal{T}}(k, p)$, for all three cases, cascade mediated by rolls is the only dominant process. In addition to the cascade process, for $T(k, p)$, as for $[Ra, Pr] = [10^8, 10]$, the energy transfer to/from the convection rolls is also relevant.

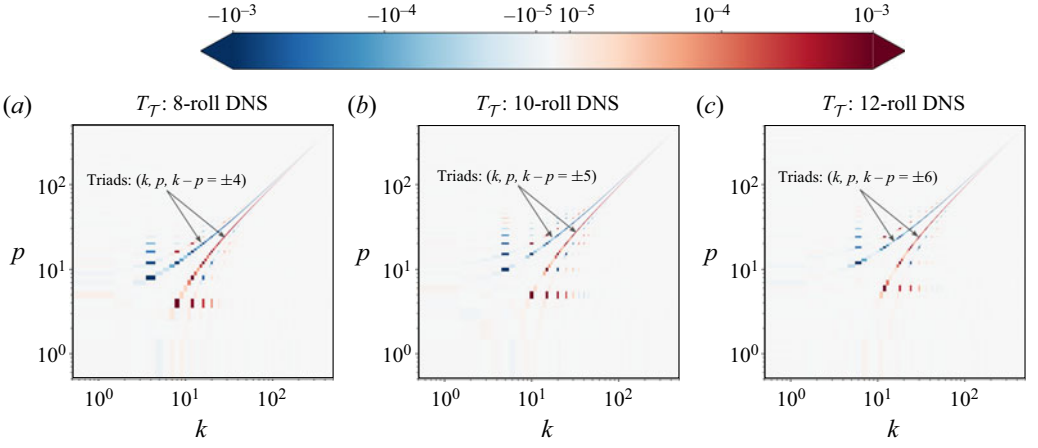

Figure 3. Scale-to-scale temperature variance transfer function $T_{\mathcal{T}}(k,\ p)$ from DNS of 2-D RBC at $[Ra,\ Pr] = [10^9,\ 3]$: (*a*) $n = 8$ state ($\Gamma_r = 1$), (*b*) $n = 10$ state ($\Gamma_r = 4/5$), (*c*) $n = 12$ state ($\Gamma_r = 2/3$). Here, k and p are the receiver and donator integer horizontal wavenumbers, respectively.

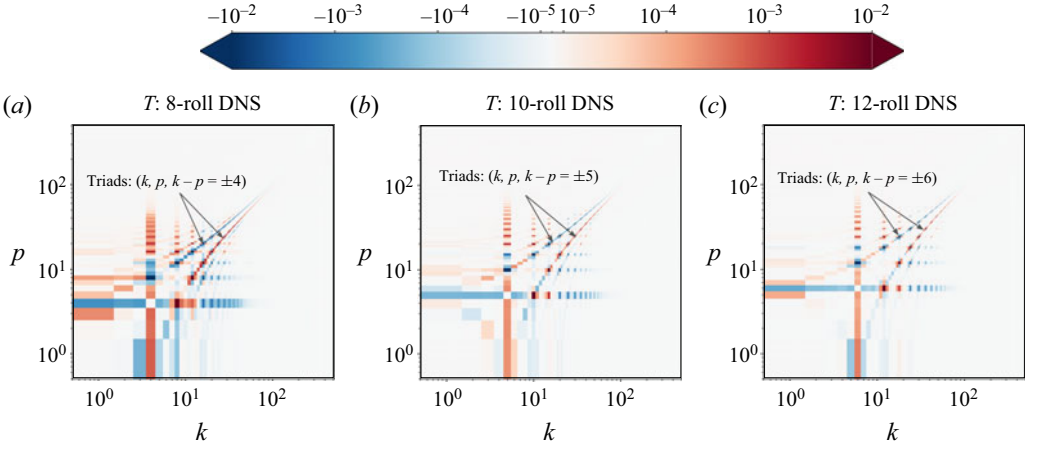

Figure 4. Scale-to-scale kinetic energy transfer function $T(k,\ p)$ from DNS of 2-D RBC at $[Ra,\ Pr] = [10^9,\ 3]$: (*a*) $n = 8$ state ($\Gamma_r = 1$), (*b*) $n = 10$ state ($\Gamma_r = 4/5$), (*c*) $n = 12$ state ($\Gamma_r = 2/3$). Here, k and p are the receiver and donator integer horizontal wavenumbers, respectively.

So in order to suppress the emergence of convection rolls of a particular value or range of Γ_r, the triad interactions involving as the mediator the target characteristic wavenumber(s) for roll formation ($k_t = [k_1, k_2, \ldots]$, say) must be removed. The forcing terms $\boldsymbol{f}$ in (2.2) and $f_{\mathcal{T}}$ in (2.3) are used to remove such triad interactions. Verma (2019) described the function of the mediator wavenumber (see chapter 4 and figure 4.3 therein, and also § 5.4.3 in Schmid, Henningson & Jankowski 2002). The role of the velocity field due to the mediator wavenumber $m = k - p$ in (2.12) and (2.13), for example, is to advect the temperature/velocity field due to the donor wavenumber p as it exchanges energy with the temperature/velocity field due to the receiver wavenumber k. The mediator wavenumber does not receive any energy in the process, and is hence named the mediator.

Because of the reality condition of the velocity field, the velocity field due to the mediator wavenumbers $m = \pm k_r$ is $\boldsymbol{u}_{k_r}$ (see (2.11)). Therefore, based on the above discussions and the expressions for the transfer functions in (2.12) and (2.13), to drop all triad interactions mediated by wavenumbers k_t, the forcing terms are defined as

$$f_{\mathcal{T}} = \textstyle\sum_{k_t} \boldsymbol{u}_{k_t} \cdot \boldsymbol{\nabla} \mathcal{T}, \tag{2.14}$$

$$\boldsymbol{f} = \textstyle\sum_{k_t} \boldsymbol{u}_{k_t} \cdot \boldsymbol{\nabla} \boldsymbol{u}. \tag{2.15}$$

The effect of the forcing terms on the OBEs in (2.1)–(2.3) may be understood by noting the overall nonlinear terms of the proposed forcing methodology, $(\boldsymbol{u} - \sum_{k_t} \boldsymbol{u}_{k_t}) \cdot \boldsymbol{\nabla} \boldsymbol{u}$ and $(\boldsymbol{u} - \sum_{k_t} \boldsymbol{u}_{k_t}) \cdot \boldsymbol{\nabla} \mathcal{T}$, in the momentum and temperature equations, respectively. As in linear/weakly nonlinear analysis, following Reynolds decomposition $\boldsymbol{u} = \boldsymbol{U}_b + \boldsymbol{u}'$ (with $\boldsymbol{U}_b = 0$ for the 2-D RBC system) and $\mathcal{T} = \mathcal{T}_b + \mathcal{T}'$, the nonlinear terms in the OBEs become

$$\left(\boldsymbol{u} - \textstyle\sum_{k_t} \boldsymbol{u}_{k_t}\right) \cdot \boldsymbol{\nabla} \boldsymbol{u} = \left(\boldsymbol{u}' - \textstyle\sum_{k_t} \boldsymbol{u}_{k_t}\right) \cdot \boldsymbol{\nabla} \boldsymbol{u}', \tag{2.16}$$

$$\left(\boldsymbol{u} - \textstyle\sum_{k_t} \boldsymbol{u}_{k_t}\right) \cdot \boldsymbol{\nabla} \mathcal{T} = \left(\boldsymbol{u}' - \textstyle\sum_{k_t} \boldsymbol{u}_{k_t}\right) \cdot \boldsymbol{\nabla} (\mathcal{T}_b + \mathcal{T}'). \tag{2.17}$$

In the above expressions, $\sum_{k_t} \boldsymbol{u}_{k_t}$ is the component of the perturbation velocity field, with $\boldsymbol{u}'$ corresponding to the chosen forcing wavenumbers k_t. Except for the forcing terms, the nonlinear terms in the perturbation equations are the same as those without forcing. Hence the forcing should in effect eliminate the linear/weakly nonlinear growth at the forcing wavenumbers k_t.

In the next section, we demonstrate that the removal of triad interactions mediated by one/multiple candidate wavenumbers by switching on $\boldsymbol{f}$ and $f_{\mathcal{T}}$ in (2.2) and (2.3) results in the emergence of convection rolls at another unforced candidate wavenumber. If all stable states are suppressed, then this forcing methodology tends to converge to flow fields with arbitrary patterns, making it a suitable method for discovering the multiple states in 2-D RBC. Additionally, the flow statistics converge much more quickly using the proposed forcing than in DNS initiated with a target roll state as in (2.8). Furthermore, using the proposed technique, the dependence of the emergence of the multiple states on the initial conditions can be bypassed for 2-D RBC.

3. Test cases

In the following, the initial conditions for the forced simulations are a $\mathcal{T}$ field consisting of random perturbations superimposed on the linear conductive profile, and $\boldsymbol{u} = 0$. We call this initial condition 'random'. The DNS are initialised either with the conditions specified in (2.8) and (2.9) (we avoid cases with $n^{(i)} \neq n$, including state transitions that take longer simulation times), or from states obtained in the forced simulations switching off the forcing.

Also in the following discussion, as obtaining accurate statistics for the roll states is not the purpose of this study, we calculate the statistics only when possible. So by the term 'convergence', we mean either the rate at which some statistical quantity (Re, for example) approaches stationarity, or obtaining the desired roll state as flow structures in a simulation that has not necessarily reached statistical stationarity.

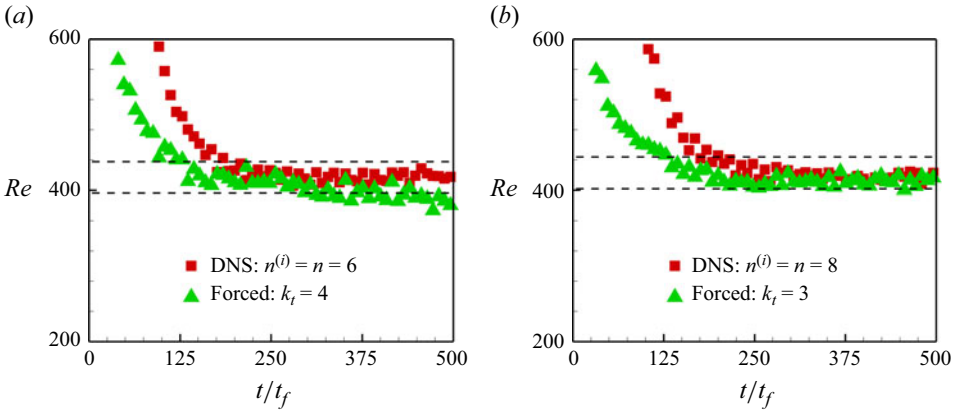

Figure 5. Plots of Re as a function of simulation time (t/t_f) from direct and forced simulations for $[Ra,\ Pr] = [10^8,\ 10]$: (a) DNS initiated with $n^{(i)} = n = 6$, and a forced simulation with $k_t = 4$; (b) DNS initiated with $n^{(i)} = n = 8$, and a forced simulation with $k_t = 3$. The horizontal dashed lines correspond to ± 5 % of the Re values reported by Wang *et al.* (2020) from their DNS.

3.1. *Multiple states for* $[Ra,\ Pr] = [10^8,\ 10]$

For $[Ra,\ Pr] = [10^8,\ 10]$, Wang *et al.* (2020) found two statistically stationary states: $n = 6$ and $n = 8$ convection rolls in a domain with $\Gamma = 8$ (mean aspect ratio of the rolls, $\Gamma_r = \Gamma/n = 4/3$ and 1, respectively). The results yielding the multiple states for this combination of control parameters are shown in figures 5 and 6.

Figures 5(a), 6(a) and 6(b) show the results from DNS initialised with $n^{(i)} = 6$ ($\Gamma_r = 4/3$), and a forced simulation with $k_t = 4$ (to suppress the emergence of the $n = 8$ state with $k_r = 4$ and $\Gamma_r = 1$). Figure 5(a) shows the convergence of Re for the two cases with simulation time t/t_f. Here, Re is used as the metric for comparison instead of Nu because of its slower convergence rate. The two simulations seem to converge at similar rates; Re computed for the two simulations converges to similar values. Figures 6(a) and 6(b) show the instantaneous snapshots of $\mathcal{T}$ at the same simulation time for the two cases considered. The forcing technique is able to capture the $n = 6$ state omitting triad interactions mediated by $k_t = 4$.

Similar conclusions may be drawn from the results obtained for $n = 8$ state in figures 5(b), 6(c) and 6(d). The DNS are initialised with $n^{(i)} = 8$, and in the forced simulation, triad interactions are removed with $k_t = 3$ as the mediator (to suppress the emergence of the $n = 6$ state with $k_r = 3$ and $\Gamma_r = 4/3$). Figure 5(b) shows that Re for the two simulations converges to similar values. Comparison of instantaneous snapshots of $\mathcal{T}$ in figure 6(c,d) show that the state $n = 8$ can also be obtained using the proposed technique that yields results similar to those of the DNS initiated with $n^{(i)} = 8$.

With the choice of appropriate k_t, the proposed forcing methodology is able to capture the multiple states for this $[Ra,\ Pr]$ combination without depending on initial conditions. The converged statistics from the simulations presented in figures 5 and 6 are tabulated in table 1. The statistics, especially Nu from the forced simulations, are in very good agreement with the DNS (these results are also in agreement with those reported by Wang *et al.* 2020). The maximum deviation of the reported Reynolds numbers is within 5 %.

What happens if both states ($n = 8$ and 6) are suppressed? Figure 7 shows an instantaneous snapshot of $\mathcal{T}$ from a forced simulation with $k_t = [3,\ 4]$ at $t/t_f = 150$. While at this t/t_f, forcing with either $k_t = 4$ or $k_t = 3$ in figure 6 yields the $n = 6$ or 8 state, respectively, for $k_t = [3,\ 4]$ the proposed technique does not yield a state with convection

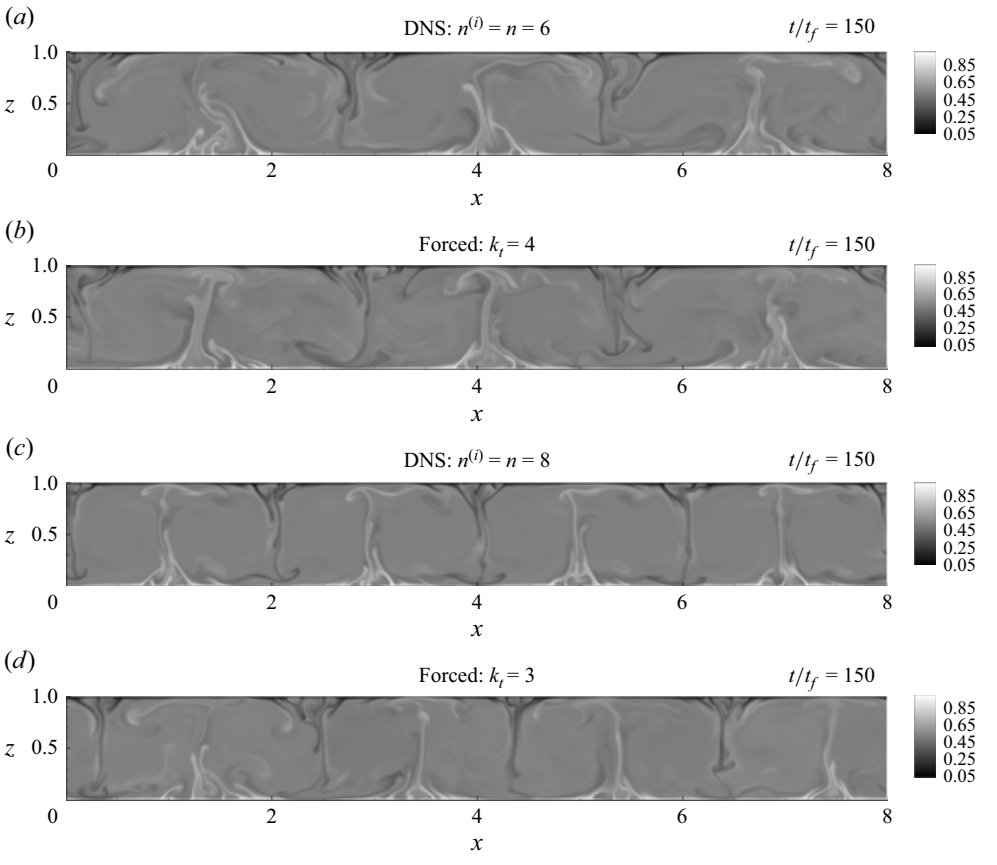

Figure 6. Instantaneous snapshots of $\mathcal{T}$ at $t/t_f = 150$ from: (*a*) DNS initiated with $n^{(i)} = n = 6$, (*b*) forced simulation with $k_t = 4$, (*c*) DNS initiated with $n^{(i)} = n = 8$, (*d*) forced simulation with $k_t = 3$.

Simulation	Initial condition: $n^{(i)}$	k_t	n	Nu	$\langle Re_x \rangle_t$	$\langle Re_z \rangle_t$
DNS	Roll state: 6	–	6	25.99	333.25	250.24
Forced	Random: –	4	6	25.79	318.26	237.95
DNS	Roll state: 8	–	8	27.59	299.42	292.61
Forced	Random: –	3	8	27.7	294.5	287.44

Table 1. Details of direct and forced simulations to capture multiple states for $[Ra, Pr] = [10^8, 10]$. Here, k_t is the integer streamwise wavenumber for forcing.

rolls of regular shape and size. Although plumes are visible, arbitrary patterns emerge without any regular shape.

3.2. *Multiple states for* $[Ra, Pr] = [10^9, 3]$

For $[Ra, Pr] = [10^9, 3]$, Wang *et al.* (2020) reported three states with different mean aspect ratios: $n = 8$ ($\Gamma_r = 1$), $n = 10$ ($\Gamma_r = 4/5$) and $n = 12$ ($\Gamma_r = 2/3$) convection rolls were obtained in a computational domain with aspect ratio $\Gamma = 8$. The results for these multiple states are presented in figures 8 and 9.

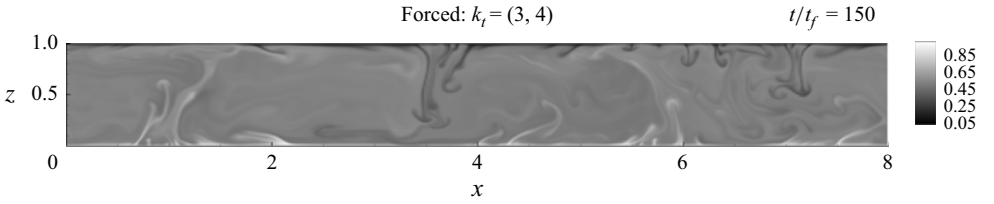

Figure 7. Instantaneous snapshot of $\mathcal{T}$ at $t/t_f = 150$ from a forced simulation with $k_t = [3, 4]$ for $[Ra,\ Pr] = [10^8, 10]$.

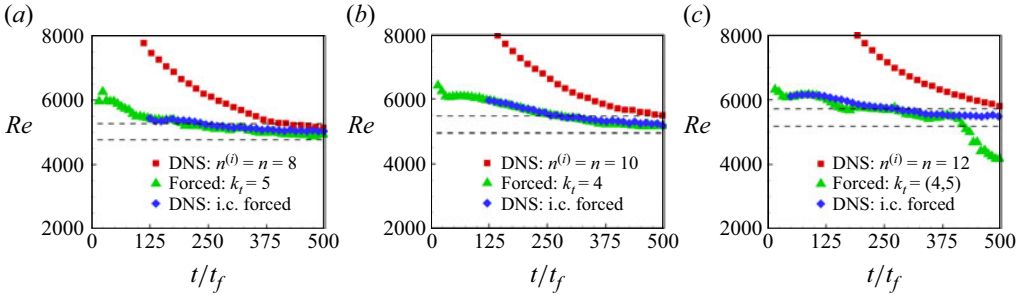

Figure 8. Plots of Re as a function of simulation time (t/t_f) for $[Ra,\ Pr] = [10^9, 3]$: (a) simulations yielding the $n = 8$ roll state, (b) simulations yielding the $n = 10$ roll state, (c) simulations yielding the $n = 12$ roll state. The cases are: DNS initiated with $n^{(i)} = n$ (red squares), forced simulation with k_t (green triangles), and switching off the forcing (blue diamonand switching off the forcing (blue diamonds). The horizontal dashed lines correspond to $\pm 5\,\%$ of the Re values reported by Wang *et al.* (2020) from their DNS. i.c. is initial condition.

Figure 8(a) shows the convergence of Re as a function of the simulation time t/t_f for DNS initiated with $n^{(i)} = 8 = n$, a forced simulation with $k_t = 5$ (suppressing emergence of $n = 10$ roll state), and essentially another DNS switching off the forcing at $t/t_f = 125$. Figures 9(a,b) show how the flow structures by plotting the instantaneous contours of $\mathcal{T}$ from the DNS and the forced simulation at $t/t_f = 68$ and 67, respectively. Clearly, the forced simulation with $k_t = 5$ has been able to capture the state with $n = 8$. In addition, starting from a random initial condition, the statistics converge much more quickly using the forcing technique in comparison to the DNS. Ideally, the forcing should be switched off once a roll state is obtained using the proposed method. Here, in figure 8(a), the result is also shown after the forcing is switched off at $t/t_f = 125$ once the $n = 8$ state is obtained in the forced simulation (blue diamond symbols). In these DNS, the $n = 8$ state obtained using the forcing was found to sustain itself even after the forcing was switched off (not shown here).

Suppression of the $n = 8$ state using $k_t = 4$, on the other hand, yields the $n = 10$ state with $\Gamma_r = 4/5$. The results from this forced simulation along with DNS initiated with $n^{(i)} = 10$ are shown in figures 8(b), 9(c) and 9(d). Figure 8(b) shows again that the convergence to a statistically stationary state is much slower in the DNS compared to the proposed method. The forcing technique yields the convection rolls as early as $t/t_f = 51$ in figure 9(d). The forcing was switched off at $t/t_f = 125$ in more DNS reported in figure 8(b). The $n = 10$ state was able to sustain itself in these DNS (not shown here).The Re statistics from this simulation are almost identical to that from the forced simulation, demonstrating the efficacy of the forcing methodology.

Suppression of both $n = 8$ and $n = 10$ roll states is necessary to yield the $n = 12$ roll state using the proposed method. The results for the roll state $n = 12$ are presented in

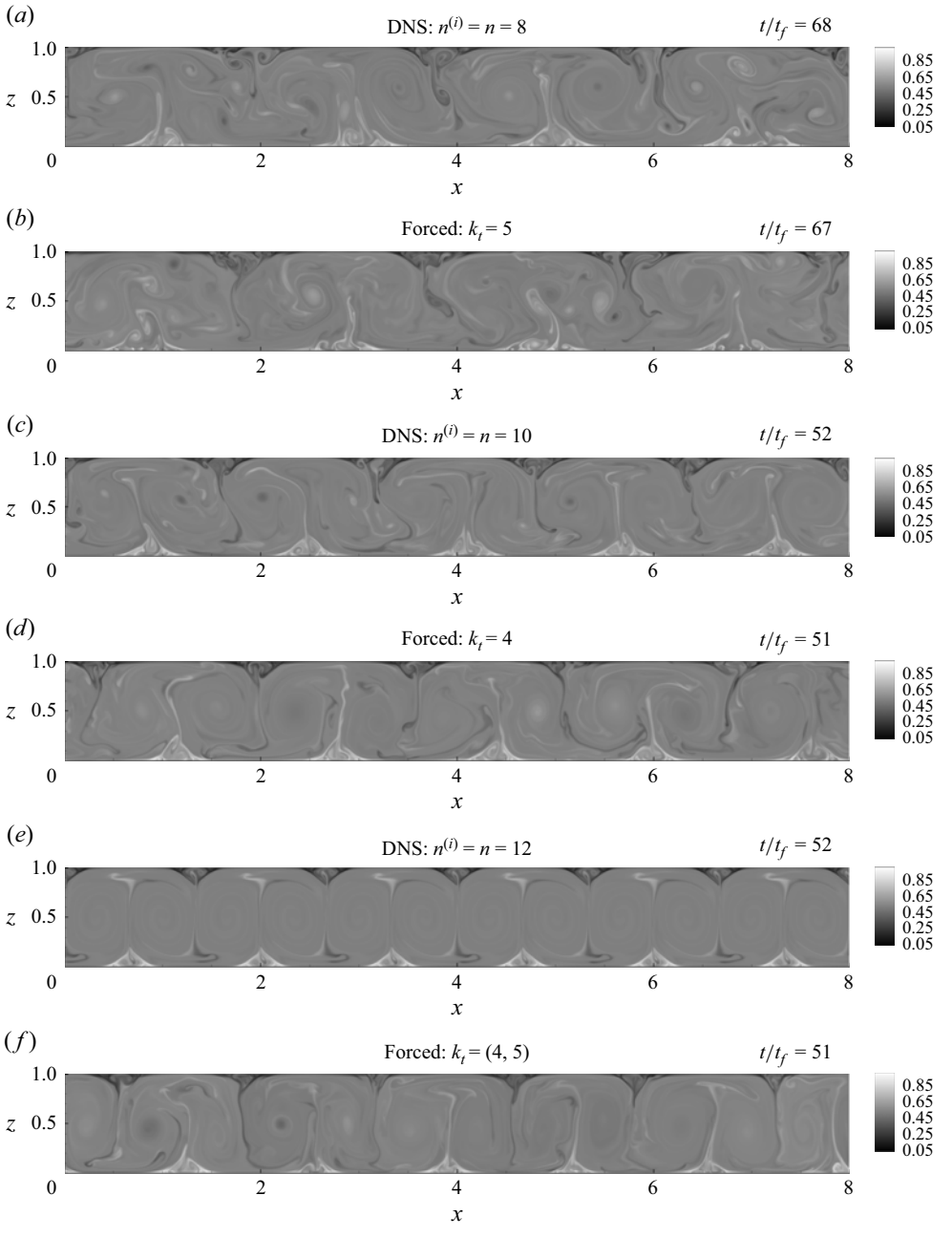

Figure 9. Instantaneous snapshots of $\mathcal{T}$ from (a,c,e) DNS initiated with $n^{(i)} = n = 8$, 10, 12, respectively, at chosen t/t_f, and (b,d,f) forced simulations with $k_t = 5$, 4, [4, 5], respectively, at chosen t/t_f.

figures 8(c), 9(e) and 9(f). The instantaneous snapshots of $\mathcal{T}$ from DNS initiated with $n^{(i)} = 12$, and a forced simulation with $k_t = [4, 5]$ (all triad interactions mediated by wavenumbers corresponding to $\Gamma_r = 1$ and 4/5 are removed), are shown in figures 9(e) and 9(f), respectively. Although initialised with a random condition, the proposed forcing technique captures the $n = 12$ state quickly, as early as $t/t_f = 51$, as shown in figure 9(f). In comparison, as reflected in the contour plot in figure 9(e), and also for Re plotted

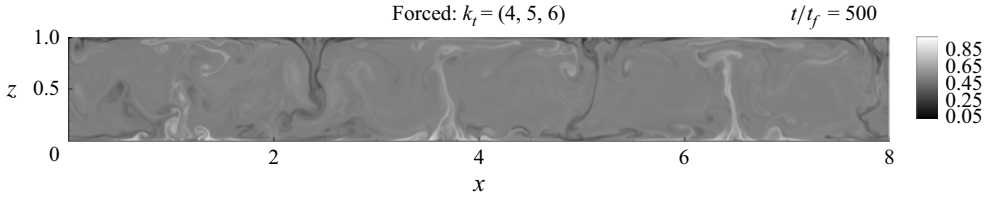

Figure 10. Instantaneous snapshot of $\mathcal{T}$ at $t/t_f = 500$ from the forced simulation with $k_t = [4, 5, 6]$ for $[Ra, Pr] = [10^9, 3]$.

against t/t_f in figure 8(*c*), the convergence of DNS initiated with $n^{(i)} = 12$ is much slower. Figure 8(*c*) also includes results from DNS after the forcing was switched off at $t/t_f = 50$. The $n = 12$ state yielded with forcing is also able to sustain itself in these DNS (not shown here). Over the course of the simulation, *Re* plotted for this simulation is also in agreement with the forced simulation.

For this $[Ra, Pr]$ combination, a forced simulation was performed suppressing known multiple states ($n = 8$, 10, 12 in a $\Gamma = 8$ computational domain). For this simulation, we chose $k_t = [4, 5, 6]$ (wavenumbers corresponding to the multiple states). The long-time solution converges to a statistically stationary $n = 6$ state (see figure 10). However, the obtained $n = 6$ state transitioned to the $n = 8$ state once the forcing was switched off (not shown here). Therefore, the proposed method can possibly lead to states that are not stable in DNS. The unphysical nature of the forcing is aggravated as more and more triad interactions are removed, or in other words, the size of the subspace, k_t, is increased. In essence, with increase in the size of the subspace k_t, the nonlinearity of the system is increasingly restricted. A forced simulation yields the most stable state (as the initial condition is 'random') of the system of equations (with restricted nonlinearity) solved that is not necessarily stable for the fully nonlinear system. The forcing terms in (2.14) and (2.15) might remove triad interactions that might otherwise be necessary for the sustenance of a state. Although the proposed method can yield the flow states and the associated statistics accurately enough to be compared with those obtained from DNS, the proposed methodology is reliant on DNS for verification purposes.

3.3. *Practical applications of the forcing technique*

The proposed method may be used to uncover the multiple convection roll states in 2-D RBC. The steps involved are as follows. (i) Perform DNS with the random initial condition to converge to a roll state (the characteristic wavenumber associated with the captured mean roll size is k_1, say). (ii) Perform simulation using the proposed forcing technique with $k_t = [k_1, \ldots]$ to test if another roll state (with characteristic wavenumber k_2, say) can be obtained. If a new state cannot be obtained, all possible states have been discovered. (iii) If another roll state is obtained, then switch off the forcing to check if the obtained state sustains in DNS. (iv) If the new roll state sustains itself in DNS, then increase the size of the subspace to $k_t = [k_1, k_2, \ldots]$, and repeat step (ii). Otherwise, if the roll state transitions back to one of the already discovered states, then all multiple states have been obtained.

Additionally, the proposed methodology can empirically designatethe stability of each of the multiple states. Ideally, the emergence of a more stable state should require suppression of a lesser number of candidate wavenumbers. The most stable state should emerge without forcing from a random initial condition, followed by other lesser stable states, with the removal of more and more triads mediated by candidate wavenumbers. When all possible multiple states are ruled out using the forcing technique, the consequent

restricted nonlinearity of the governing equations may yield highly unstable states that are otherwise unlikely to emerge for the fully nonlinear system (see Bose *et al.* 2024).

We emphasise that the proposed method could possibly be used to compute the different states in other flow configurations where multiple states exist for a set of control parameters. The continuation based methods (Dijkstra *et al.* 2014) can yield a superposition of multiple states at such a point in the bifurcation diagram, while only one of the states is obtained as the solution is continued along a branch. On the other hand, the present method should be able to capture the multiple states as discrete solutions at such a point in the bifurcation diagram, provided that the wavenumbers associated with the dominant flow structures mediate energy in triad interactions. The investigation of such possibilities remains an open question.

4. Conclusions

In this paper, a new methodology is proposed to obtain the multiple convection roll states in 2-D RBC flow. For the same control parameters $[Ra, Pr]$, convection rolls with different aspect ratios (Γ_r) emerge yielding different statistically stationary states; in previous works, the selection of Γ_r was dependent on Γ_r of rolls in the initial condition. Using the methodology proposed in this paper, the possible multiple states for any $[Ra, Pr]$ combination can be captured exhaustively, circumventing the issues related to the dependence of the emergence of the states on initial conditions.

In the proposed method, forcing terms are prescribed that remove select nonlinear triadic scale interactions from the OBEs (2.1)–(2.3). This is motivated by the observation that the characteristic horizontal wavenumber associated with the mean size of the convection rolls (k_r) mediates temperature variance and kinetic energy transfer processes in triad interactions at a statistically stationary state establishing cascade processes (figures 1 and 2). The participating wavenumbers in such triads are of the form $[k, p, m = k - p = \pm k_r]$, where, k, p and m are the receiver, donator and mediator wavenumbers, respectively. Herein, we prescribed the forcing terms in (2.14) and (2.15), leveraging this information to remove triad interactions that are mediated by one/multiple target wavenumbers, $k_t = [k_1, k_2, \ldots]$. Removing such triad interactions physically suppresses the emergence of the convection rolls with characteristic wavenumbers k_t. As a consequence, roll formation is encouraged at another candidate wavenumber that does not belong to k_t, which is therefore allowed to mediate energy among triads and establish the essential cascade processes.

The proposed forcing technique is used to obtain the multiple states in a computational domain with aspect ratio $\Gamma = 8$ for two cases – $[Ra, Pr] = [10^8, 10]$ and $[10^9, 3]$. For both these cases, the multiple states could be yielded from a 'random' initial condition that does not include any signature of the final roll state. For comparison, we also perform DNS initialised from momentum fields bearing the signature of the target roll states (2.8) and (2.9). The two possible states for $[Ra, Pr] = [10^8, 10]$ are captured by suppressing in each case the mediation of energy by one of the candidate wavenumbers for roll formation (figures 5 and 6). Additionally, the statistics obtained from the forced simulations are in good agreement with the statistics obtained from the DNS (table 1). Removing the triad interactions mediated by both candidate wavenumbers does not capture any roll state with a regular pattern (figure 7). All three multiple states could also be captured for $[Ra, Pr] = [10^9, 3]$ – suppression of only one candidate wavenumber was sufficient to yield two of the multiple states. The $n = 8$ state could be captured suppressing the emergence of $n = 10$ state, and vice versa (figures 8(*a*,*b*) and 9(*a*–*d*)). However, to capture the $n = 12$ state, candidate wavenumbers corresponding to both $n = 8$ and $n = 10$ states had to be forced out (figures 8(*c*) and 9(*e*,*f*)). All the multiple states captured using the

proposed method were found to sustain themselves in direct simulations after the forcing was switched off. If all three states are suppressed, then the forcing technique yields an $n = 6$ state – a state that was found to transition to the $n = 8$ state once the forcing was switched off. Specifically, for $[Ra,\ Pr] = [10^9,\ 3]$, the forcing technique converges to the statistically stationary states much more quickly than in DNS initiated with the signature of the target states.

It has been demonstrated that the proposed methodology could be utilised to uncover all possible multiple roll states in 2-D RBC efficiently. The possible states obtained by the forcing technique, while 'stable' for the forced system of equations, are not necessarily stable for the original unforced system of equations (e.g. the $n = 6$ state obtained for the forced system for $[Ra,\ Pr] = [10^9,\ 3]$). The proposed forcing method yields a roll state quickly, irrespective of the initial condition; the forced simulations also approach statistical stationarity much more quickly. In addition, the proposed method can designate each state with respect to its stability and in comparison to other states. However, it must be noted that despite capturing the states quickly, this method is reliant on the direct simulation for verification, as ultimately it uses manipulation of the triadic scale interactions, which are unphysical in nature. Even if a state appears stable under the forced equations, DNS must be run with that state as the initial condition to verify its true stability. We believe that the proposed method should be able to discretely capture the multiple states in other flow configurations in both non-turbulent and turbulent regimes provided that the dominant flow structures mediate energy in triadic scale interactions.

Funding. We gratefully acknowledge financial support from the Max Planck Society, the German Research Foundation (DFG), from grants 521319293, 540422505 and 550262949. We also thank the HPC systems of Max Planck Computing and Data Facility (MPCDF) for the allocation of computational time.

Declaration of interests. The authors report no conflict of interest.

Data availability statement. The data that support the findings of this study will be available upon reasonable request.

References

Ahlers, G., Grossmann, S. & Lohse, D. 2009 Heat transfer and large scale dynamics in turbulent Rayleigh–Bénard convection. *Rev. Mod. Phys.* **81** (2), 503–537.

Bodenschatz, E., Pesch, W. & Ahlers, G. 2000 Recent developments in Rayleigh–Bénard convection. *Annu. Rev. Fluid Mech.* **32** (1), 709–778.

Bose, R., Kannan, V. & Zhu, X. 2024 The generalized quasilinear approximation of two-dimensional Rayleigh–Bénard convection. *J. Fluid Mech.* **998**, A52.

Boullé, N., Dallas, V. & Farrell, P.E. 2022 Bifurcation analysis of two-dimensional Rayleigh–Bénard convection using deflation. *Phys. Rev. E* **105** (5), 055106.

Broecker, W.S., Peteet, D.M. & Rind, D. 1985 Does the ocean–atmosphere system have more than one stable mode of operation? *Nature* **315** (6014), 21–26.

Burns, K.J., Vasil, G.M., Oishi, J.S., Lecoanet, D. & Brown, B.P. 2020 Dedalus: a flexible framework for numerical simulations with spectral methods. *Phys. Rev. Res.* **2** (2), 023068.

Buzzicotti, M., Bhatnagar, A., Biferale, L., Lanotte, A.S. & Ray, S.S. 2016 Lagrangian statistics for Navier–Stokes turbulence under Fourier-mode reduction: fractal and homogeneous decimations. *New J. Phys.* **18** (11), 113047.

Chillà, F. & Schumacher, J. 2012 New perspectives in turbulent Rayleigh–Bénard convection. *Eur. Phys. J. E* **35** (7), 1–25.

Cortet, P.-P., Chiffaudel, A., Daviaud, F. & Dubrulle, B. 2010 Experimental evidence of a phase transition in a closed turbulent flow. *Phys. Rev. Lett.* **105** (21), 214501.

Dijkstra, H.A. 2014 Numerical bifurcation methods and their application to fluid dynamics: analysis beyond simulation. *Commun. Comput. Phys.* **15** (1), 1–45.

Faranda, D., Sato, Y., Saint-Michel, B., Wiertel, C., Padilla, V., Dubrulle, B. & Daviaud, F. 2017 Stochastic chaos in a turbulent swirling flow. *Phys. Rev. Lett.* **119** (1), 014502.

FAVIER, B., GUERVILLY, C. & KNOBLOCH, E. 2019 Subcritical turbulent condensate in rapidly rotating Rayleigh–Bénard convection. *J. Fluid Mech.* **864**, R1.
FAVIER B., SILVERS L.J. & PROCTOR M.R.E. 2014 Inverse cascade and symmetry breaking in rapidly rotating Boussinesq convection. *Phys. Fluids* **26** (9), 096605.
FRISCH, U., POMYALOV, A., PROCACCIA, I. & RAY, S.S. 2012 Turbulence in noninteger dimensions by fractal Fourier decimation. *Phys. Rev. Lett.* **108** (7), 074501.
HUISMAN, S.G., VAN DER VEEN, R.C.A., SUN, C. & LOHSE, D. 2014 Multiple states in highly turbulent Taylor–Couette flow. *Nat. Commun.* **5** (1), 3820.
KRUG, D., LOHSE, D. & STEVENS, R.J.A.M. 2020 Coherence of temperature and velocity superstructures in turbulent Rayleigh–Bénard flow. *J. Fluid Mech.* **887**, A2.
LANOTTE, A.S., MALAPAKA, S.K. & BIFERALE, L. 2016 On the vortex dynamics in fractal Fourier turbulence. *Eur. Phys. J. E* **39** (4), 1–8.
LI, J., SATO, T. & KAGEYAMA, A. 2002 Repeated and sudden reversals of the dipole field generated by a spherical dynamo action. *Science* **295** (5561), 1887–1890.
LOHSE, D. & SHISHKINA, O. 2024 Ultimate Rayleigh–Bénard turbulence. *Rev. Mod. Phys.* **96** (3), 035001.
PANDEY, A., SCHEEL, J.D. & SCHUMACHER, J. 2018 Turbulent superstructures in Rayleigh–Bénard convection. *Nat. Commun.* **9** (1), 2118.
VAN DER POEL, E.P., STEVENS, R.J.A.M., SUGIYAMA, K. & LOHSE, D. 2012 Flow states in two-dimensional Rayleigh-Bénard convection as a function of aspect-ratio and Rayleigh number. *Phys. Fluids* **24** (8), 085104.
RAVELET, F., MARIÉ, L., CHIFFAUDEL, A. & DAVIAUD, F. 2004 Multistability and memory effect in a highly turbulent flow: experimental evidence for a global bifurcation. *Phys. Rev. Lett.* **93** (16), 164501.
REETZ, F. & SCHNEIDER, T.M. 2020 Invariant states in inclined layer convection. Part 1. Temporal transitions along dynamical connections between invariant states. *J. Fluid Mech.* **898**, A22.
REETZ, F., SUBRAMANIAN, P. & SCHNEIDER, T.M. 2020 Invariant states in inclined layer convection. Part 2. Bifurcations and connections between branches of invariant states. *J. Fluid Mech.* **898**, A23.
SCHMEITS, M.J. & DIJKSTRA, H.A. 2001 Bimodal behavior of the Kuroshio and the gulf stream. *J. Phys. Oceanogr.* **31** (12), 3435–3456.
SCHMID, P.J., HENNINGSON, D.S. & JANKOWSKI, D.F. 2002 *Stability and Transition in Shear Flows*.
SCHUMACHER, J. & SREENIVASAN, K.R. 2020 Colloquium: unusual dynamics of convection in the sun. *Rev. Mod. Phys.* **92** (4), 041001.
SHRAIMAN, B.I. & SIGGIA, E.D. 1990 Heat transport in high-Rayleigh-number convection. *Phys. Rev. A* **42** (6), 3650–3653.
STEVENS, R.J.A.M., BLASS, A., ZHU, X., VERZICCO, R. & LOHSE, D. 2018 Turbulent thermal superstructures in Rayleigh–Bénard convection. *Phys. Rev. Fluids* **3** (4), 041501.
VAN DER VEEN, R.C.A., HUISMAN, S.G., DUNG, O.-Y., TANG, H.L., SUN, C. & LOHSE, D. 2016 Exploring the phase space of multiple states in highly turbulent Taylor–Couette flow. *Phys. Rev. Fluids* **1** (2), 024401.
VERMA, M.K. 2019 *Energy Transfers in Fluid Flows: Multiscale and Spectral Perspectives*. Cambridge University Press.
WANG, Q., VERZICCO, R., LOHSE, D. & SHISHKINA, O. 2020 Multiple states in turbulent large-aspect-ratio thermal convection: what determines the number of convection rolls? *Phys. Rev. Lett.* **125** (7), 074501.
WANG, Q., WAN, Z.-H., YAN, R. & SUN, D.-J. 2018 Multiple states and heat transfer in two-dimensional tilted convection with large aspect ratios. *Phys. Rev. Fluids* **3** (11), 113503.
WEEKS, E.R., TIAN, Y., URBACH, J.S., IDE, K., SWINNEY, H.L. & GHIL, M. 1997 Transitions between blocked and zonal flows in a rotating annulus with topography. *Science* **278** (5343), 1598–1601.
XI, H.-D. & XIA, K.-Q. 2008 Flow mode transitions in turbulent thermal convection. *Phys. Fluids* **20** (5), 055104.
XIA, K.-Q., HUANG, S.-D., XIE, Y.-C. & ZHANG, L. 2023 Tuning heat transport via coherent structure manipulation: recent advances in thermal turbulence. *Natl. Sci. Rev.* **10** (6), nwad012.
YANG, Y., CHEN, W., VERZICCO, R. & LOHSE, D. 2020 Multiple states and transport properties of double-diffusive convection turbulence. *Proc. Natl Acad. Sci. USA* **117** (26), 14676–14681.
ZIMMERMAN, D.S., TRIANA, S.A. & LATHROP, D.P. 2011 Bi-stability in turbulent, rotating spherical Couette flow. *Phys. Fluids* **23** (6), 065104.